DOE/ER/40304--6

DE90 011185

FINAL REPORT

PARITY VIOLATING WEAK NEUTRAL CURRENT EFFECTS IN ELASTIC e-^{12}C SCATTERING

Department of Energy Grant Number DE-FG02-86ER40304

for the Period

August 15, 1987 - May 14, 1989

DISCLAIMER

Michael S. Lubell
Department of Physics
City College of CUNY
April 25, 1990

Historically, parity nonconservation (PNC) experiments have played a significant role in furthering our understanding of the electroweak interaction. For example, prior to the development of electroweak unification, PNC observations in β-decay served as a major test of the V-A theory.[1] More recently, PNC measurements in deep-ineleastic electron-deuteron scattering[2] served as a benchmark test for neutral current processes predicted by the Standard Model and helped validate the SU(2)xU(1) structure of electroweak unification. These seminal studies relied heavily on electron polarization to generate PNC signatures.

Today, the rich structure of neutral currents continues to provide polarized electron experiments with great potential for further exploration. Extensions of the Standard Model and the specifics of weak hadronic currents are two obvious candidates for such applications. Some of the potential studies, however, assume extremely difficult proportions because they must be carried out at small values of the four-momentum transfer, Q^2, in order that the relevant form factors remain large. Since PNC asymmetries are typically proportional to Q^2, the experiments of interest will be characterized by asymmetries that may be as small as 10^{-6} or 10^{-7}.

Recently we completed a measurement of the PNC asymmetry in elastic e-^{12}C scattering at the Bates Electron Accelerator Center in which we achieved a precision at the level of approximately 10^{-7}, an improvement of a factor of five beyond that of the best previous experimental result.[3] Moreover, the asymmetry we determined,

$$A \equiv \frac{\sigma_R - \sigma_L}{\sigma_R + \sigma_L}, \qquad (1)$$

where σ_R and σ_L represent the differential cross sections for the scattering of electrons with right and left helicity respectively, unlike the quantities determined in many other PNC experiments, suffers no ambiguity in the thecretical interpretation of its meaning, a result which follows from the spinless, isoscalar nature of the ^{12}C nucleus.[4] These properties permit the relevant nuclear physics in the elastic $e^{-12}C$ interaction to be described by a single form factor, which cancels precisely in the asymmetry given by Eq. (1).

Within the context of a four-fermion interaction picture, the PNC asymmetry of Eq. (1) for $e^{-12}C$ elastic scattering may be expressed as[4,5]

$$A = \frac{3G_F}{2\sqrt{2}\ \pi\alpha}\ \tilde{\Upsilon}\ Q^2, \tag{2}$$

where G_F is the Fermi coupling constant, α is the fine structure constant, and $\tilde{\Upsilon}$ is the PNC coupling constant[6] for an axial-vector coupling to the electron and an isoscalar coupling to the constituents of the hadrons. The Standard Model, which characterizes all PNC coupling constants in terms of a single parameter, provides the concise relationship

$$\tilde{\Upsilon} = \frac{2}{3}\ \sin^2\theta_W, \tag{3}$$

where θ_W is the weak mixing angle. The currently accepted value[7] of 0.2327 ± 0.0015 for $\sin^2\theta_W$ obtained from a variety of other experiments leads to a value of 0.155 ± 0.001 for $\tilde{\Upsilon}$. The most precise PNC measurement[8] of $\tilde{\Upsilon}$ currently relies heavily on a study of atomic cesium[9] which unfortunately requires the accurate calculation[10] of complex atomic wave functions in order

to extract $\tilde{\gamma}$ from the experimentally measured quantities. For this reason and for reasons related to the important role that $\sin^2\theta_W$ and hence $\tilde{\gamma}$ play in our understanding of electroweak unification, we undertook the determination of $\tilde{\gamma}$ by a different method, one which does not rely on elaborate theoretical modeling.

Our experiment utilized kinematic conditions determined by an electron energy of 250 MeV and a scattering angle of 35^o, for which Q takes on the value 150 MeV/c. Based upon the accepted value of $\sin^2\theta_W$, the predicted asymmetry is $A = 1.89 \times 10^{-6}$. Since our electron polarization, P_e, was only 0.37, we had to be prepared to measure an experimental asymmetry, $A_{exp} = P_e A$, of only 0.70×10^{-6}, a value so small that it placed severe demands on the experimental apparatus, in terms of both statistical precision and control of systematic uncertainties. Specifically we required an intense polarized electron beam with properties that remained essentially invariant under helicity reversal. In order to meet these demands, we found it necessary to devote substantial effort to the development of GaAs photoemission[11] technology as well as to the precise control of helicity reversal of circularly polarized laser light. In addition we expended considerable effort on the control and monitoring of the energy, position, and intensity of the accelerated electron beam.

A schematic diagram of the experiment appears in Fig. 1. The polarized electron source,[12] which served as the injector for the MIT/Bates electron accelerator, is described in detail in Appendix A. In brief, circularly polarized light from a cw Kr-ion laser, electro-optically modulated to match the 1% duty factor of the accelerator, produced polarized electrons by photoemission from a GaAs <100> crystal which had been prepared with Cs and NF_3 to generate a negative electron affinity. The resulting high quantum

efficiency (1.5 - 3%) allowed us to maintain average electron currents of 30-60 μA on target with the use of modst cw laser power (1-2 W). During experimental runs, we operated the source at a repetition rate of 600 Hz with a pulse length of 16 μs, conditions which resulted in a typical e-folding crystal lifetime of 12-18 h. The extracted electron beam, accelerated to 320 keV prior to injection, was characterized by an electron polarization of 0.37 ± 0.02 (as determined from 24 separate Mφller scattering[13] measurements) and a helicity-correlated stability of ~ 10^{-5}. An illustration of the polarized electron source, mounted in its high-voltage Faraday cage, is shown in Fig. 2.

We controlled the helicity of the electron beam on a pulse to pulse basis by applying positive and negative voltage pulses to a Pockels cell located in the optics train as shown in Fig. 3. We also employed a rotatable half-wave retardation plate, located upstream from the Pockels cell, to provide an independent means of reversing the beam helicity. Since the Bates accelerator frequency of 600 Hz was locked to the a.c. line voltage, we divided our data into 10 "timeslots" corresponding to the 60 Hz subharmonics. In order to set a helicity pattern for a given orientation of the half-wave plate, we then generated 10 random helicities, one for each timeslot, followed by a complemented set of helicities for the succeeding 10 beam pulses. We repeated this procedure every 20 pulses, thus enabling us to compute asymmetries for individual, randomly chosen pulse-pairs associated with a given time slot.

In order to monitor the characteristics of the high-energy electron beam we employed seven toroids to measure the intensity, four profile monitors in front of the ^{12}C target to determine the incident position and angle, and one position monitor at a point where the beam was dispersed in momentum to analyze the energy. As shown schematically in Fig. 1, the high-energy beam impinged on a 5-g/cm^2 target with the elastically scattered electrons focused

onto Lucite Cerenkov detectors by a pair of single-quadrupole spectrometers. Since approximately 10^5 electrons were detected during each beam pulse, we did not employ individual event counting but rather signal integration followed by 16-bit ADC recording.

Our accumulated data filled 307 magnetic-tape reels, each reel corresponding to a 30 minute data run. With the 10 timeslots handled independently, we were thus able to divide each reel into 10 "miniruns" for each of which we were then able to calculate an asymmetry and an associated uncertainty based upon standard statistical treatment. A histogram of the parity violating asymmetry for the 3,070 independent miniruns is shown in Fig. 4 together with the expected distribution based upon Gaussian statistics. Approximately 1% of the data were deleted from this plot by loose cuts that trapped for aberrant accelerator behavior. The excellent agreement between the remaining 99% of the data shown and the expected Gaussian distribution lead us to claim excellent understanding of our statistical uncertainties.

For the measurement of an asymmetry at the 10^{-7} level, great care clearly must be exercised in the determination of systematic errors. For our experiment, helicity-correlated beam parameters such as intensity, energy, position, and angle constituted the most obvious and most important class of systematic errors. The first of these arose because the intensity of laser light transmitted to the photocathode depended slightly on helicity, thereby causing the electron intensity to depend slightly on helicity. Accelerator beam-loading effects then converted the intensity correlation into an energy correlation, the latter producing a spurious asymmetry through the strong dependence of electromagnetic cross sections on energy. The correlations of beam position and angle with helicity arose because the position of the laser beam on the photocathode also depended slightly on helicity, thereby causing

the envelope of electron trajectories to depend slightly on helicity. The resulting position and angle correlations produced spurious asymmetries through the dependence of the spectrometer acceptances on both the position and angle of the beam incident on the target.

In order to achieve a satisfactory degree of control over these systematic effects, we both minimized the helicity correlations at the electron source during data acquisition and corrected our measured asymmetries with the use of position monitor data during data analysis. We found that the largest potential source of correlation was produced by a polarization-induced transport asymmetry (PITA)[12,14] in the intensity of the circularly polarized laser light. Explained in detail elsewhere, the PITA effect arises because of slight deviation from the ideal Pockels cell voltage required for perfect quarter-wave retardation introduces a small degree of ellipticity into the nominal circular polarization of the laser light. Since the transmission of elliptical polarized light through an optical system generally depends upon the orientation of the principal axis of the ellipse, left and right handed beams will suffer differing amounts of attenuation, thus giving rise to a helicity dependent intensity of light incident on the GaAs crystal. By calculating the intensity asymmetry on-line every 3 minutes, we were able to correct the Pockels cell voltage appropriately thereby producing an intensity asymmetry that averaged to more than approximately 1 ppm during a run. During the course of our initial studies, we found that application of voltage to the Pockels cell also produced slight deflections in the laser beam. However, through careful alignment of the Pockels cell[15] and with the use of a lens system that provided point-to-point focusing of the Pockels cell onto the crystal, we were able to suppress this effect.

In order to correct our data for any remaining helicity correlated effects, we ramped the beam steering coils during data acquisition and used the beam monitors to determine a set of correction coefficients, $\{a_i\}$, appropriate to both angular and positional deviations of the beam on target. (Typical values of a_i were < 10 ppm/μm.) We then corrected our raw asymmetries, A_{raw}, to obtain the desired experimental asymmetries, A_{exp}, according to the prescription

$$A_{exp} = A_{raw} - \Sigma\,(a_i)\,(\delta M_i), \tag{4}$$

where $\{\delta M_i\}$ is the set of helicity-correlated beam-monitor differences which typically had values of less than 0.1 μm. Since the accelerated electron beam was generally characterized by large fluctuations in current, we had sufficient inherent "noise" in the beam-loaded energy spectrum to carry out a correlation analysis applicable to the coefficient involving energy. We checked the energy correlation analysis with the use of an energy vernier located on one of the accelerator klystrons.

As a further means of detecting and hence eliminating systematic effects, we introduced a half-wave retardation plate into the optical chain which provided an independent means of reversing the helicity of the laser light. With this device, which we employed periodically at lengthy intervals, we were able to reverse the sign of the PNC asymmetry without altering the contributions of most of the undesirable systematic helicity-correlated effects. By combining data for alternate half-wave plate settings, we were thus able to suppress the effects of systematic helicity-correlations at a very small level. We point out that during the development of the experiment, we paid special attention to the need for eliminating electronic cross talk

that might have resulted from the high-voltage pulses applied to the Pockels cell. To that end we avoided ground loops wherever possible and employed timing in the electronics that placed communications out of phase with data acquisition.

From a comparison of the difference in the asymmetries separately measured by the left and right spectrometers, we were able to place limits on the contributions due to transverse components of the electron polarization. From other studies we were also able to conclude that systematic effects arising from electronic non-linearities, beam phase-space differences, and scattering from magnetized ion shielding were all small. We summarize the various systematic corrections to the raw asymmetry in Table 1, along with their estimated uncertainties. We note that with the exception of those due to energy and position correlations, all correction terms were negligible. Insofar as energy and position are concerned, the root mean square value arising from monitor differences was only 0.3 ppm per run and only 0.04 ppm for the entire data sample. We also point out that the asymmetry difference between the two spectrometers was only 0.14 ± 0.14 ppm and that the asymmetry difference between the results for the two half-wave plate settings was 0.04 ± 0.14 ppm. Thus we have extremely high confidence in our PNC result.

With the systematic corrections applied we obtain[16] a value of $0.60 \pm 0.14 \pm 0.02$ ppm for A_{exp}, where the first uncertainty is purely statistical and the second, systematic. With the beam polarization, P_e, taken as 0.37 ± 0.02, the correction factors due to inelastic nuclear levels[17] and neutrons taken respectively as 1.00 ± 0.01 and 0.98 ± 0.02, and the average effective Q^2 taken as $(1.00 \pm 0.02)\ Q_o^2$, Q_o being the calculated ideal kinematic value, we obtain a value of $0.136 \pm 0.032 \pm 0.009$ for the value of $\tilde{Y}$. This result is consistent with the prediction of the Standard Model given earlier. We note in

conclusion, that the high precision which we achieved in our studies has prepared the way for even higher accuracy measurements that might be achieved in the future if higher data rates can be achieved. The use of larger acceptance spectrometers and longer running times conceivably could improve the statistical accuracy to the level of ± 1%. With theoretical uncertainties including hadronic contributions to radiative corrections,[18] parity admixtrures in nuclear states,[19] and isospin mixing[20] expected to contribute well below this level, such future work should prove extremely interesting.

REFERENCES

1. T.D. Lee and C.N. Yang, Phys. Rev. **104**, 254 (1956); C.S. Wu et al., Phys. Rev. **105**, 1413 (1957).
2. C.Y. Prescott et al., Phys. Lett. **84B**, 524 (1979).
3. W. Heil et al., Nucl. Phys. **B327**, 1 (1989).
4. G. Feinberg, Phys. Rev. D **12**, 3575 (1975).
5. J.D. Walecka, Nucl. Phys. **A285**, 349 (1977).
6. P.Q. Hung and J.J. Sakurai, Ann. Rev. Nucl. Part. Sci. **31** (1981).
7. S. Fanchiotti and A. Sirlin, Phys. Rev. D **41**, 319 (1990).
8. U. Amaldi et al., Phys. Rev. D **36**, 1385 (1987).
9. M.C. Noecker et al, Phys. Rev. Lett. **61**, 310 (1988).
10. W. Johnson et al., Phys. Rev. A **37**, 1395 (1988); V.A. Dzuba et al., Phys. Scr. **36**, 69 (1987); C. Bouchiat and C.A. Piketty, Europhys. Lett. **2**, 511 (1986).
11. D.T. Pierce and F. Meier, Phys. Rev. B **13**, 5484 (1976).
12. G.D. Cates et al., Nucl. Instr. Meth. **A278**, 293 (1989).
13. C. Møller, Ann. Physik **14**, 531 (1933); P.S. Cooper et al., **34**, 1589 (1975).
14. G.D. Cates et al., Opt. Comm., to be submitted.
15. K. Kumar, Ph.D. Thesis, Syracuse University, 1990.
16. P.A. Souder et al., Phys. Rev. Lett., submitted.
17. R. Michaels, Ph.D. Thesis, Yale University, 1988.
18. W.J. Marciano and A. Sirlin, Phys. Rev. D **27**, 552 (1983); **29**, 75 (1984).
19. B.D. Serot, Nucl. Phys. **A322**, 408 (1979).
20. T.W. Donnelly et al., Nucl. Phys. **A503**, 589 (1989).

FIGURE CAPTIONS

FIG. 1 Schematic diagram of the Bates parity experiment. The broken section of the beam line indicates the interposition of the linear accelerator.

FIG. 2 Layout of the GaAs polarized electron source. Showing (1) Faraday cage, (2) gun chamber, (3) preparation chamber, (4) extraction airlock, (5) accelerator column, (6) magnetically coupled manipulators, (7) focusing solenoid, (8) SF_6 pressure vessel aluminum housing, (9) SF_6 pressure vessel fiberglass insulated housing, (10) porcelain insulators, (11) steel I-beam supports, (12) aluminum corona rings, (13) beam pipe, (14) ion pumps, and (15) Ti-sublimation pump.

FIG. 3 Schematic diagram of optics system including a krypton-ion laser (Kr^+), a helium-neon laser (HeNe), an electro-optical "shutter," and a "flipper" for reversing the helicity of the laser beam. The optical elements are labeled as follows: (PC) Pockels cell, (P) glan air-spaced prism polarizer (L) lens, (M) mirror, (BS) beam splitter, (D) photodiode, (S) iris field-stop, ($\lambda/2$) half-wave retardation plate, and (BC) Babinet-Soleil compensator. The folded path was used for set-up purposes as well as PITA-effect monitoring.

FIG. 4 Histogram of asymmetry, A_i, normalized to its statistical error, σ_i, for each of 3070 miniruns. The solid curve is a Gaussian of unit variance with an area equal to the number of miniruns.

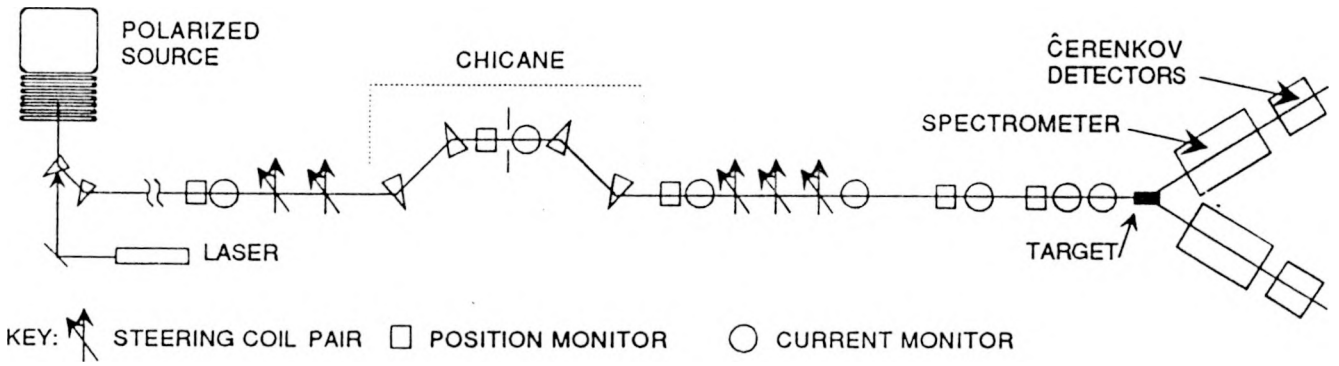
POLARIZED
SOURCE
CHICANE
ČERENKOV
DETECTORS
SPECTROMETER
LASER
TARGET
KEY:
STEERING COIL PAIR
POSITION MONITOR
CURRENT MONITOR

FIG. 1

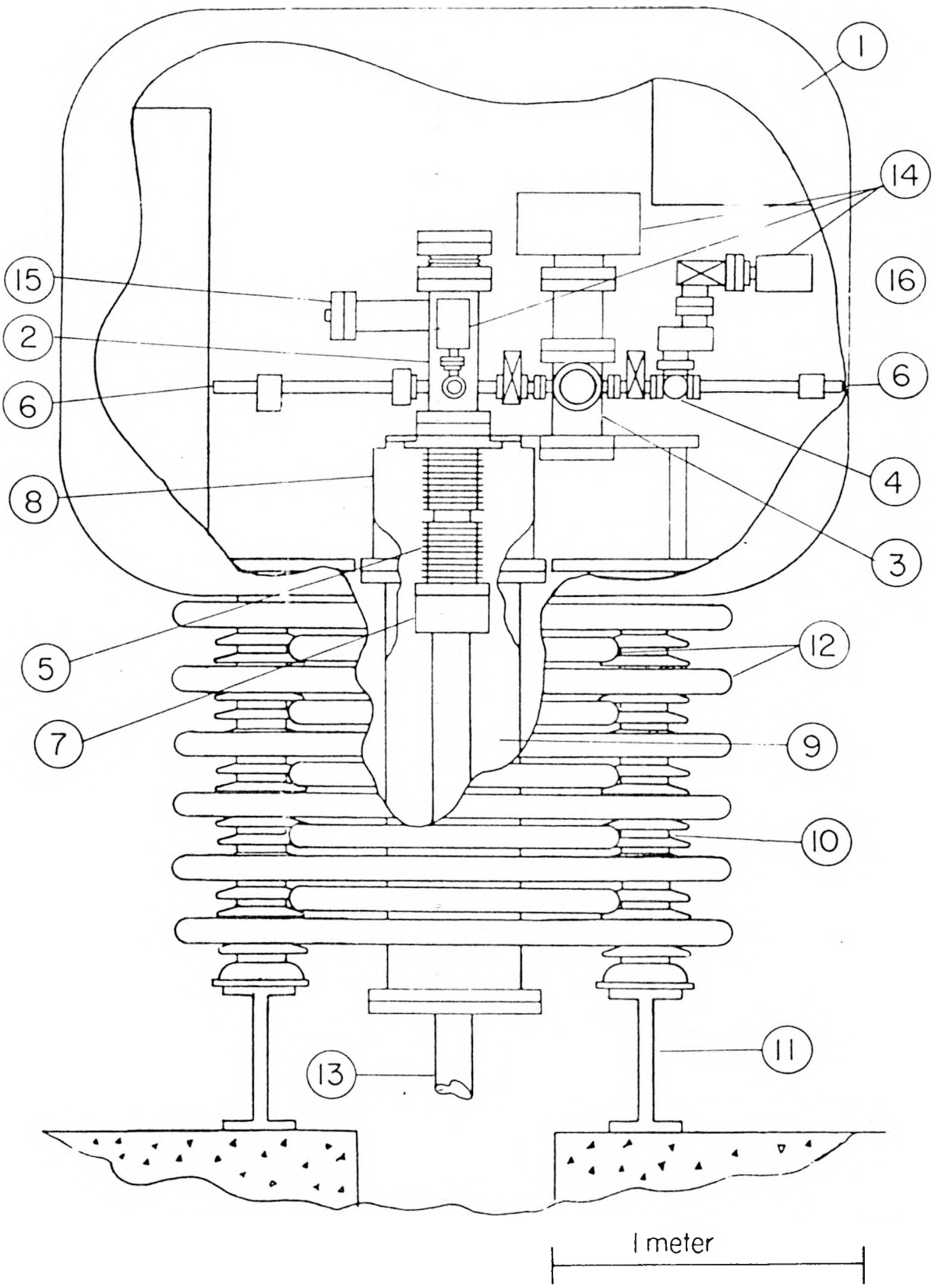

FIG. 2

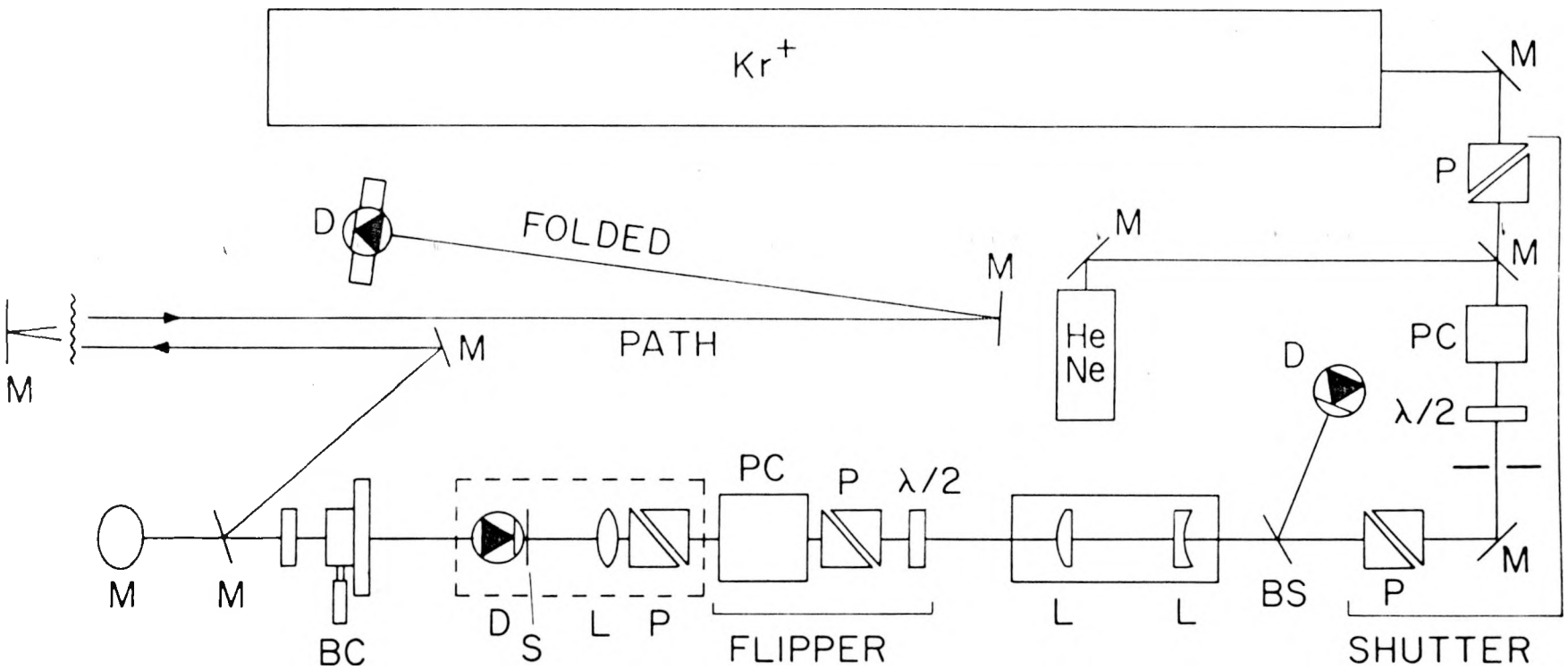
Kr+
M
P
D
FOLDED
M
M
M
M
PATH
He
Ne
PC
D
λ/2
M
M
PC
P
λ/2
M
M
BC
D
S
L
P
FLIPPER
L
L
BS
P
M
SHUTTER

FIG. 3

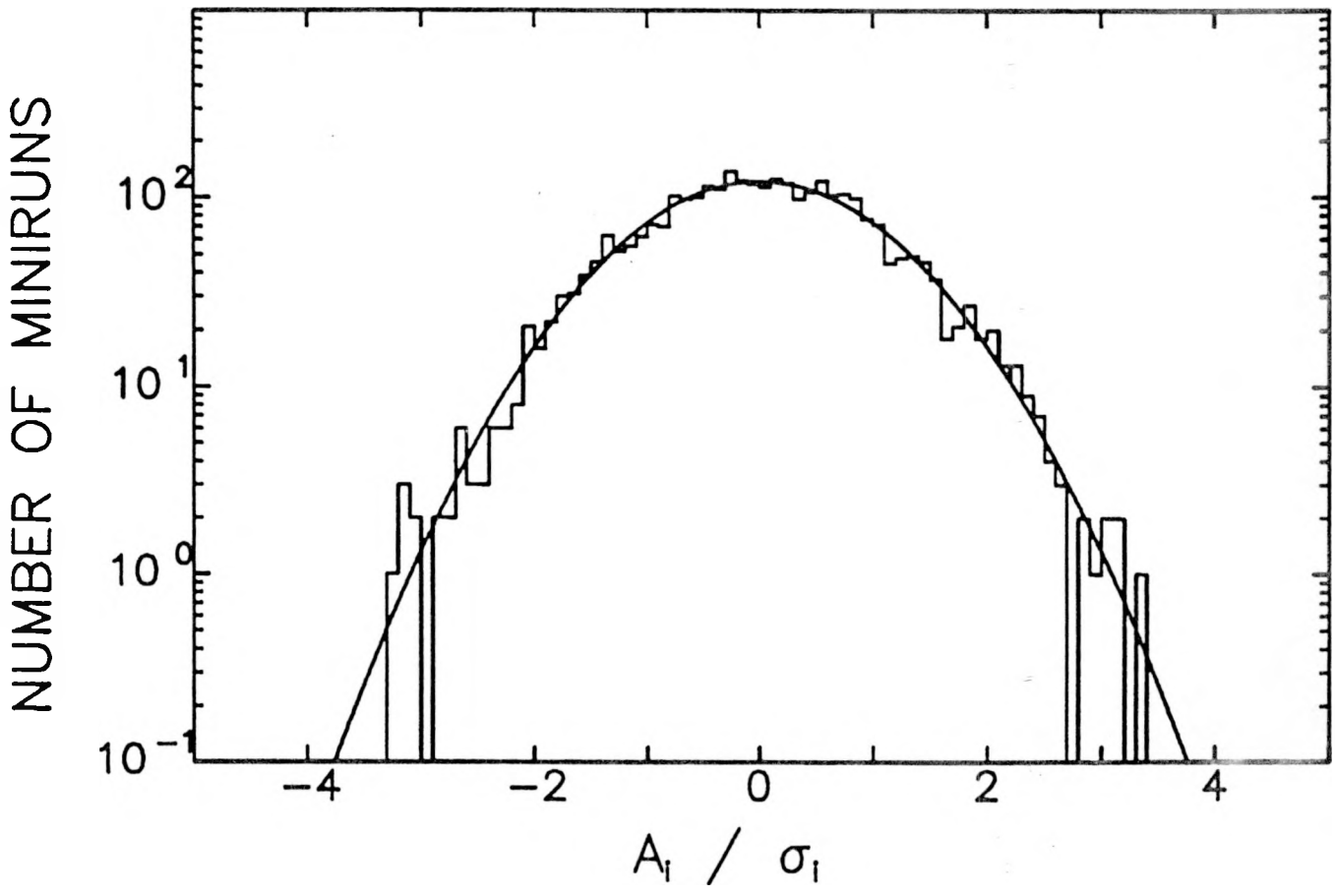

FIG. 4